

RSC Advances

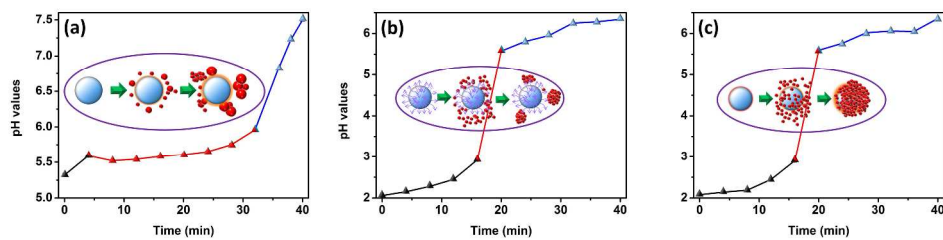


This is an *Accepted Manuscript*, which has been through the Royal Society of Chemistry peer review process and has been accepted for publication.

Accepted Manuscripts are published online shortly after acceptance, before technical editing, formatting and proof reading. Using this free service, authors can make their results available to the community, in citable form, before we publish the edited article. This *Accepted Manuscript* will be replaced by the edited, formatted and paginated article as soon as this is available.

You can find more information about *Accepted Manuscripts* in the [Information for Authors](#).

Please note that technical editing may introduce minor changes to the text and/or graphics, which may alter content. The journal's standard [Terms & Conditions](#) and the [Ethical guidelines](#) still apply. In no event shall the Royal Society of Chemistry be held responsible for any errors or omissions in this *Accepted Manuscript* or any consequences arising from the use of any information it contains.



693x179mm (150 x 150 DPI)

ARTICLE

Al₂O₃/Yttrium-compound core-shell structure formation with burst nucleation: a process driven by electrostatic attraction and high surface energy

Cite this: DOI:

Received 00th January 2012,
Accepted 00th January 2012

DOI: 10.1039/x0xx00000x

www.rsc.org/

Daidong Guo,^{a,†} Lili Zhao,^{a,†} Yuanhua Sang,^{a,*} Hong Liu,^{a,*} Shaohong Liu,^b and Xudong Sun^b

A partial wet chemical route, by inducing Al₂O₃ nanoparticles into Y(NO₃)₃ solution to form a core-shell structured yttrium aluminum garnet (YAG) precursor based on burst nucleation synthesis process, was studied intensively. By simulating the reaction conditions with urea and NH₄HCO₃ as precipitants, a two-step formation mechanism with different dynamic processes is proposed to describe the core-shell structure formation process. During the most of the whole process, the electrostatic attraction between the opposite surface charges of Al₂O₃ and Y-compound nanoparticles is deemed to one apparent driven force. However, the high surface energy of Y-compound nanoparticles originated from the burst nucleation process plays a key role to complete the core-shell structure formation. The as-obtained precursor can transform into pure YAG nanoparticle, retaining the morphology of the template Al₂O₃, which is of high quality for preparing transparent ceramics. The full understanding of the mechanism can make this route a novel method to synthesize core-shell nanostructured binary oxide precursor.

Introduction

Binary oxides have attracted much attention because of their broad applications and substantial application prospects. For example, LaMnO₃ is used as electrolyte of solid-oxide fuel cell,¹ Y₃Fe₅O₁₂ is used as laser alignment, microwave devices, and is also important foundational material of circulator, phase shifter, modulator, etc.,² Transparent MgAl₂O₄ ceramic is an excellent optical material in ultraviolet, visible and infrared bands used as bow cap and window material,³ and so on. Materials with proper nanoparticle morphology are usually essential to realize their high performances. Therefore, morphology controllable synthesis of the complex oxides has been a hot topic.^{4,5} As one of the most attractive materials, yttrium aluminum garnet (YAG) nanoparticles has been extensively studied in order to get a well-controlled morphology, such as sol-gel method^{6,7}, homogeneous precipitation^{8,9}, co-precipitation methods^{10,11}, microwave irradiation^{12,13} and solvothermal methods^{14,15}, etc. In practice, morphology control of Y-Al precursor is difficult because of the hydrolysis character of Al³⁺ ions which induces the formation of flocculated sediment during the co-precipitation process.¹⁶ For instance, the YAG precursor nanoparticles with

gradient distribution of Y/Al elements is obtained by adding the NH₄HCO₃ solution into the Y-Al solution in droplet, while that with hollow morphology is formed by adding the Y-Al solution into the NH₄HCO₃ solution.¹⁷ Moreover, many factors, such as the precipitant application, reactant concentration, reaction temperature, rate of reaction, and even ambient humidity during the synthesis of YAG precursor, can affect the morphology and composition control.¹⁷⁻²⁰ Thus, it is difficult to mass-produce YAG nanopowders with uniform size distribution, less aggregation, and precise chemical composition. Contrastively, spherical nanosized particle of individual Y₂O₃ with uniform size distribution is easy to be synthesized through a homogeneous precipitation process.^{21,22} In addition, monodispersed commercial Al₂O₃ nanopowders with high quality is available. For controlling the morphology of the YAG precursor with good dispersion, a core-shell structure, which Al₂O₃ nanoparticles as the core and Y-compound as the shell, seems to be a good choice. The most common approaches for core-shell structure are chemical synthesis²³, chemical vapor deposition²⁴, laser-induced assembly²⁵, electrostatic attraction²⁶ etc. In our route, we proposed a method to synthesis spherical YAG nanoparticles by assembling a layer of Y-compound on

Al_2O_3 nanoparticle to form a $\text{Al}_2\text{O}_3/\text{Y}$ -compound core-shell nanostructure, and then transformed into YAG nanoparticles through a micro-solid state reaction.²⁷ The main idea of our route lies in the self-assembling of Y-compound on the surface of Al_2O_3 nanoparticles based on burst nucleation synthesis process, and the advantages of this route has been discussed. Based on the first understanding of the basic idea for this partial wet chemical route, and inspired by the full understanding for extensive application, we will discuss the formation mechanism of core-shell YAG precursor intensively in the current work. The fundamental of the self-assembled core-shell precursors is studied by sorting the reaction process into two stages: first is the pre-coating process of Y-compound on the Al_2O_3 nanoparticle surface driven by electrostatic attraction; second is the assembling of tiny Y-compound nanoparticles formed in the burst nucleation process onto the pre-coated Al_2O_3 nanoparticle surface, principally driven by its high surface energy. By the full understanding of the formation of YAG core-shell nanostructured precursor, this partial wet chemical route can be applied in the synthesis of many other core-shell nanostructured binary oxides.

Experimental

The typical experimental procedure for the synthesis of the YAG core-shell precursor via the partial wet route is as follows.²⁷ $\text{Y}(\text{NO}_3)_3 \cdot 6\text{H}_2\text{O}$ (Alfa Aesar, 99.99%), $\alpha\text{-Al}_2\text{O}_3$ nanopowders (size of 100–200 nm, Taimei Chemicals Co., Ltd, 99.99%) were well dispersed in deionized water by ultrasonication to form a stoichiometric ($\text{Y}/\text{Al}=3/5$) suspension liquid. The concentration of Y^{3+} was kept at 0.015 mol/L throughout the process. Urea (Sinopharm Chemical Reagent Co., Ltd, Specpure) with the ratio of urea/ Y^{3+} in 20/1 was applied as precipitant. After homogenizing at room temperature, the mixed liquid was heated at 90 °C for 3 h with stirring. Besides, surface modified Al_2O_3 with polyacrylic acid (PAA) or ammonium polyacrylate (PAA- NH_4) as surfactants were used instead of pure Al_2O_3 nanoparticles to study the effect of the surface modification of Al_2O_3 on the core-shell structure formation. The concentration of surfactants were all 100 ppm in the reaction system. The experiment with individual Al_2O_3 has also been performed in the absence of Y^{3+} with urea solution. To simulate the slow reaction rate during the precipitation process, the NH_4HCO_3 solution (0.2 M, Sinopharm Chemical Reagent Co., Ltd, Specpure) was used as precipitant by adding into the suspension mixed as-above in droplet. All the precursors obtained with those methods were collected by filtration. Then they were washed with deionized water and ethanol to remove byproducts and inhibit hard-agglomeration, respectively. After drying in the oven at 80 °C for 24 h, the powders were obtain for characterization. Some samples were reserved during the reaction process to discuss the intermediate state of the core-shell structure formation (Mid-products). For ceramics sintering, the YAG-precursor powders were sieved and then calcined at 1250 °C for 2 h. The calcined powders were uniaxially pressed into pellets under 50

MPa and followed by cool isostatic pressing under 200 MPa. Then they were sintered at 1780 °C for 4 h in 4×10^{-3} Pa vacuum in the furnace with a tungsten heating element (712-T, Thermal Technology LLC, USA).

The pH of the suspension was monitored with a pH meter with an accuracy of 0.02 (PHS-3D, Leici, China). A zeta potential analyzer (Zetapals, Brookhaven Instruments Corporation, USA) was used to characterize the electrokinetic properties of the powders. A powder suspension of 0.1 mg/mL concentration was prepared in deionized water for the zeta potential measurement. Fourier transform infrared (FTIR) analysis on the YAG precursor was performed by an IR spectrometer (NEXUS 670, American Thermo Nicolet Company) over the range of 4000–400 cm^{-1} . X-ray powder diffraction (XRD) patterns of the powders were recorded on a Bruker D8 Advance powder X-ray diffractometer with $\text{Cu K}\alpha$ ($\lambda=0.15406$ nm). The morphology of the powder and synthesized samples were characterized by a field emission scanning electron microscope (FESEM, S-4800, HITACHI, Japan). The core-shell structure of precursor materials was investigated by a high resolution transmission electron microscope (HRTEM, JEM-2100F, JEOL, Japan). The distribution of elements of the powder was studied using energy-dispersive X-ray spectrometer (EDS) attached to the HRTEM. The residual Y^{3+} in the filtration solution was checked with an inductively coupled plasma emission spectrometer (ICP-AES, IRIS Intrepid II XSP, Thermo Electron Corporation, USA) to make sure the stoichiometry of the YAG precursor.

Results and discussion

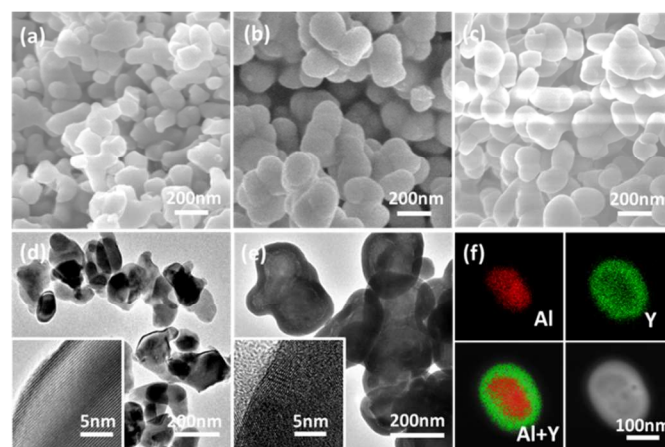


Fig. 1 SEM images of the samples: (a) the pure Al_2O_3 , (b) $\text{Al}_2\text{O}_3/\text{Y}$ -compound precursor, and (c) YAG particles calcined at 1250 °C of the $\text{Al}_2\text{O}_3\text{-Y}(\text{NO}_3)_3\text{-Urea}$ system; TEM image of the samples: (d) the pure Al_2O_3 with the HRTEM image inset, (e) $\text{Al}_2\text{O}_3/\text{Y}$ -compound precursor with the inset of the HRTEM image of Y-compound precursor shell, (f) EDS element mapping data of Al, Y and Al+Y, as well as the TEM image in dark field.

Fig. 1 shows the SEM and TEM images of $\alpha\text{-Al}_2\text{O}_3$, $\text{Al}_2\text{O}_3/\text{Y}$ -compound precursor and the calcined YAG particles synthesized by the partial wet-chemical process using urea as precipitant, as well as the EDS mapping results of the

precursor. As shown in Fig. 1(a), the Al_2O_3 nanoparticles are of smooth surface with a homogeneous size distribution around 130 nm. After the precipitation process, the YAG precursor (Fig. 1(b)) shows a rough surface in size of 250 nm. Measured by ICP-AES, the residual Y ions in the filtration solution is very little, indicating a full precipitation of Y ions during the reaction (Table S1, supporting information). By calcination at 1250 °C for 2 h, pure YAG nanoparticles are obtained identified by the XRD results (Fig. S1, supporting information), and the powder (Fig. 1(c)) exhibits a similar morphology to that of the YAG precursor in sizes of 170 nm, but with regular surface even better than that of the pure Al_2O_3 . The TEM image of the pure Al_2O_3 confirms the well dispersibility of Al_2O_3 nanoparticles and the inset shows the lattice image of the pure $\alpha\text{-Al}_2\text{O}_3$ confirming its high crystallization (Fig. 1(d)). It implies that the Al_2O_3 nanoparticles are good to work as templates. The core-shell structure of the YAG precursor is noted in the TEM image and the EDS mapping results (Fig. 1(e,f)). The as-obtained precursor particles exhibit an obvious interface between the core and shell, which corresponds to the different composition in the core and shell structures. And the lattice image of Y-compound precursor shell (inset of Fig. 1(e)) shows its polycrystal character. In addition, it is notable that the shell structure is easily affected by the electron exposure (Fig. S2, supporting information). Compared with the morphology of the pure $\alpha\text{-Al}_2\text{O}_3$, the shell composition is different from the center. It indicates that $\text{Al}_2\text{O}_3/\text{Y}$ -compound core-shell structure should be formed with the Al_2O_3 core and Y-compound shell. The EDS mapping results give a direct evidence for the core-shell structure formed by the Al_2O_3 and Y-compound respectively. It is clear that Al element is in the core position with Y element surrounding. Consistently, blocked by the Y-compound shell, the XRD intensity of Al_2O_3 is decreasing with an increase of Y-compound shell (Fig. S1). It is notable that this core-shell structure with Y-compound shell restricts the neck-sintering between the neighbor YAG particles at a certain temperature due to the high melting points of Y-rich compounds, leading to a good dispersibility.²⁷ The highly transparent ceramics (Fig. S3 in the supporting information) were obtained by sintering at 1780 °C in the vacuum of 4×10^{-3} Pa. It demonstrates the high quality of the YAG powders, which indicates that the YAG-precursor powders with good sintering properties can be synthesized via a partial wet chemical route.

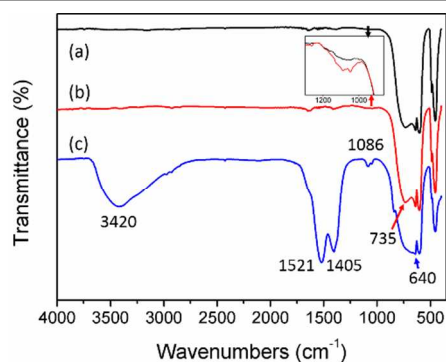


Fig. 2 FTIR spectra of the pure Al_2O_3 (curve a), mid-product (curve b), YAG precursor (curve c) in $\text{Al}_2\text{O}_3\text{-Y}(\text{NO}_3)_3\text{-Urea}$ system.

The assembling process of the Y-compound nanoparticles on the surface of Al_2O_3 nanoparticle are very important to understand the formation mechanism of $\text{Al}_2\text{O}_3/\text{Y}$ -compound core-shell nanostructures. As reported previously, Y-compound nuclei can be formed abruptly in $\text{Y}(\text{NO}_3)_3$ urea solution with a temperature over 83 °C²⁸, which is called as a burst nucleation process. Normally, the Y-compound nuclei can form uniform spherical nanoparticles by self-assembling. To study the formation mechanism of the $\text{Al}_2\text{O}_3/\text{Y}$ -compound core-shell structure in the $\text{Al}_2\text{O}_3\text{-Y}(\text{NO}_3)_3\text{-Urea}$ system intensively, the chemical bands evolution under various conditions were discussed by the FTIR measurement. As shown in Fig. 2, the FTIR spectra of $\alpha\text{-Al}_2\text{O}_3$ (curve a), the mid-product obtained from the suspension at the reaction temperature of 80 °C (pH=2.6, curve b) and the precursor particle obtained after holding at 90 °C for 3 h (pH=6.8, curve c) are different. The absorption bands in range of 800–400 cm^{-1} , which are mainly attributed to metal-oxygen lattice vibration, are identified in the FTIR spectra of pure Al_2O_3 (curve a). The main peaks at 450, 600, 640 and 735 cm^{-1} are assigned to the characteristic Al-O vibrations.²⁹ The band at 1640 cm^{-1} is corresponding to water (H_2O) adsorption. After the system being heated up to 80 °C, the FTIR spectra of the collected Al_2O_3 (Mid-product) (curve b) shows no obviously difference from that of the pure Al_2O_3 . However, the enlarged spectra in region 800–1300 cm^{-1} shows some peaks around 1086 cm^{-1} become stronger than that of the pure Al_2O_3 (inset of Fig. 2). These peaks are assigned to the C-O bond stretching vibration.³⁰ It implies that the Al_2O_3 surface has been modified by some kinds of carbonate precipitant or precipitate, and it is consistent with the individual study of Al_2O_3 with NH_4HCO_3 (Fig. S4 in the supporting information). As shown in the FTIR spectra of YAG precursor obtained after reaction at 90 °C for 3 h (curve c), some peaks become much stronger, and some new peaks appear. The broad peak centered at 3420 cm^{-1} corresponds to the stretching mode of the hydroxyl groups ($-\text{OH}$).³¹ The peaks at 850 cm^{-1} and at ~ 1085 , ~ 1405 and ~ 1530 cm^{-1} are originated from C-O bond bending and stretching vibration, respectively.³² As looking into the band in the range of 400–800 cm^{-1} mainly attributed to metal-oxygen lattice vibration, it is notable that the peak between 735 and 640 cm^{-1} has significantly enhanced. Considering the peak at ~ 730 cm^{-1} is the characteristic Al-O vibration, and as being known, heavy atom substitution will reduce the metal-oxygen vibration frequency, which exhibits as red-shift in IR absorption, so the peak between 735 and 640 cm^{-1} can be assigned as the Y-O vibration. These peaks should be corresponding to the formation of Y-compound.

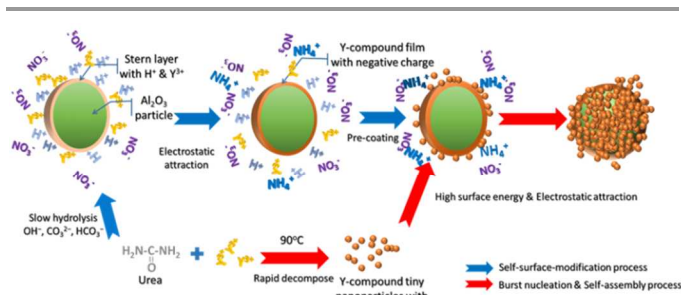


Fig. 3 The sketch of the core-shell structure formation in $\text{Al}_2\text{O}_3\text{-Y}(\text{NO}_3)_3\text{-Urea}$ system.

Based on the above results, the formation of the core-shell structure is proposed and illustrated in Fig. 3. At the beginning of urea hydrolysis, the precipitant groups of OH^- , CO_3^{2-} and HCO_3^- are generated, which modifies the surface of template particle ($\alpha\text{-Al}_2\text{O}_3$ core). These groups should be attributed to the slow decomposition of urea below 83°C . The layer of these groups could attract Y ions on the surface of $\alpha\text{-Al}_2\text{O}_3$ template in reaction system. As reported previously, $\text{Y}(\text{OH})\text{CO}_3 \cdot x\text{H}_2\text{O}$ is formed in the suspension with the urea hydrolysis.^{28,33} However, restricted by the competition of crystal nucleation and growth related to the concentration of $\text{Y}(\text{OH})\text{CO}_3 \cdot x\text{H}_2\text{O}$, the Y ions on the Al_2O_3 surface is considered easily forming the precipitate. This is a pre-coating process of the Al_2O_3 nanoparticles with Y-compound. When urea rapidly decomposes above 83°C , large amount of negative ion groups (HCO_3^- , OH^- , etc.) will increase sharply and react quickly with Y^{3+} to form Y-compound nuclei, which is assigned to be the burst nucleation process, and then the Y-compound nuclei assemble on the surface of Al_2O_3 nanoparticle, and form a shell on Al_2O_3 nanoparticle. It means the core-shell structure formation process consists of two stages, the pre-coating with Y-compound on the surface of Al_2O_3 nanoparticles and the shell structure formation occurs following a burst nucleation process. To make the process of the individual stage clear, the specific experiments are designed and proceeded accordingly.

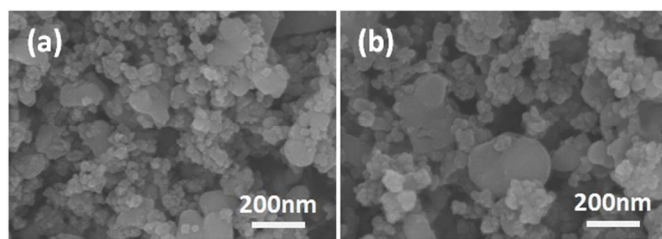


Fig. 4 SEM images of the YAG precursors obtained in $\text{Al}_2\text{O}_3\text{-Y}(\text{NO}_3)_3\text{-Urea}$ system with (a) PAA and (b) PAA- NH_4 as surfactants, respectively.

Table 1 Zeta potentials of the samples in $\text{Al}_2\text{O}_3\text{-Y}(\text{NO}_3)_3\text{-Urea}$ system.

Samples	ζ (mV)
Pure Al_2O_3	46.1±1.9
Mid-product*	32.7±0.7
Y-compound	-28.5±2.1
YAG precursor**	-5.7±1.7
Al_2O_3 with PAA	-44.5±0.6
Al_2O_3 with PAA- NH_4	-46.8±0.7

* Obtained at pH=2.6; ** Obtained at pH=6.8.

Surface modified Al_2O_3 with PAA and PAA- NH_4 were performed to check the effect of the organic surfactant on the formation of $\text{Al}_2\text{O}_3/\text{Y}$ -compound core-shell structures. As shown in Fig. 4, the SEM images exhibit that both of the precursors obtained with PAA (Fig. 4(a)) and PAA- NH_4 (Fig. 4(b)) have large particles in sizes of 100–200 nm and small particles in sizes of 10–50 nm. Because the Al_2O_3 nanoparticles used as templates are larger than 100 nm, the particles smaller than 50 nm should be identified as the newly formed Y-compounds. It indicates that the morphology of the as-obtained YAG precursor with PAA and with PAA- NH_4 are all failed in the formation of core-shell structure. Considering with the success in core-shell structure formation without PAA or PAA- NH_4 , the surface charge modification and the self-assembly process should be different with the addition of organic surfactants. The surface charge property evolution of samples can give some information to probe into the formation process. So the surface charge properties of the $\alpha\text{-Al}_2\text{O}_3$ particle in $\text{Al}_2\text{O}_3\text{-Y}(\text{NO}_3)_3\text{-urea}$ suspension, the $\text{Al}_2\text{O}_3/\text{Y}$ -compound particle obtained at pH=2.6, the $\text{Al}_2\text{O}_3/\text{Y}$ -compound particle obtained at pH=6.8, the individual Y-compound, as well as the $\alpha\text{-Al}_2\text{O}_3$ particle with PAA and with PAA- NH_4 were analyzed in forms of zeta potential (Table 1). The zeta potential of original $\alpha\text{-Al}_2\text{O}_3$ powder is 46.1±1.9 mV. When Al_2O_3 nanoparticles are dispersed in urea solution and the solution is heated below 83°C , the zeta potential drops to about 37 mV, which is caused by the adsorption of negative ions (HCO_3^- , OH^- , etc.) demonstrated in previous section. The measured zeta potential of Y-compound particles (obtained via the homogeneous precipitation method) is about -28.5 mV, which indicates that Al_2O_3 nanoparticles and Y-compound nanoparticles possess opposite charges. It should supply the driven force for the core-shell structure assembling at the beginning. With the increase of the shell thickness, the effect of the electrostatic attraction becomes weak, which can not support the assembling process any more. Then, the high surface energy of the tiny Y-compounds originated from the burst nucleation process should act as the main driven force for the formation of core-shell structure completely. The small zeta potential value of YAG precursor (-5.7 mV) should be due to the compensation of the opposite charges from the two different nanoparticles. However, after surface modification with PAA and PAA- NH_4 , Al_2O_3 nanoparticles show high negative zeta potential values of -44.5±0.6 mV and -46.8±0.7 mV, respectively. The electrostatic repulsion between these Al_2O_3 nanoparticles and Y-compounds in the suspension corresponds

to the failure of core-shell structure formation. As illustrated in Fig. 5, the main effect of the surface modification with PAA or PAA-NH₄ lies in the cutting off of the assembling process.

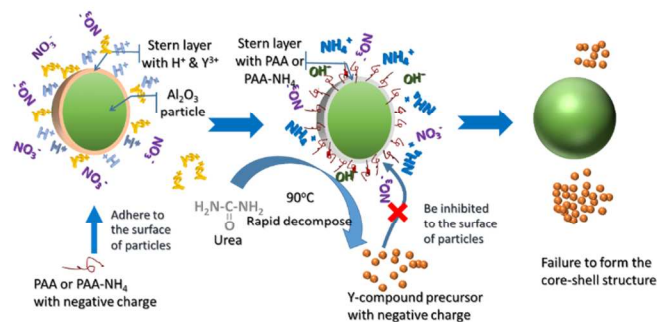


Fig. 5 The sketch of reaction process in Al₂O₃-Y(NO₃)₃-Urea system with PAA or with PAA-NH₄ as surfactants.

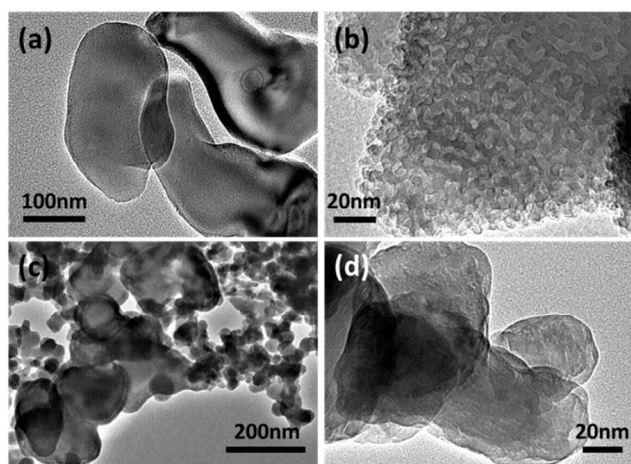


Fig. 6 Morphology of the samples in Al₂O₃-Y(NO₃)₃-NH₄HCO₃ system: (a) TEM images of the mid-product obtained at pH=3.5, (b) and the magnitude image with high electron explore; (c) TEM images of YAG precursor obtained at pH=6.8, (d) and its magnitude image.

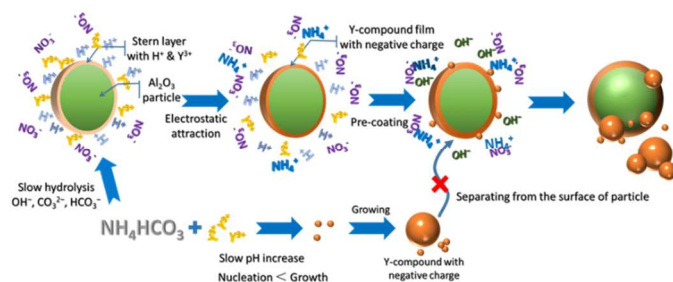


Fig. 7 The sketch of reaction process in Al₂O₃-Y(NO₃)₃-NH₄HCO₃ system.

To clarify the proposed mechanism of core-shell structure formation, an experiment with NH₄HCO₃ as precipitant was designed to simulate a similar reaction process but with a slow reaction rate. The dropwise-adding of NH₄HCO₃ to Al₂O₃-Y(NO₃)₃ suspension is performed to realize a slow pH evolution (Fig. S5, supporting information), and the morphology of the as-obtained samples are shown in Fig. 6. The pH of the as-prepared Al₂O₃-Y(NO₃)₃ suspension is about

1.5. By adding NH₄HCO₃ solution into the suspension, the pH approaches to 3.5. The morphology of the as-obtained mid-product (pH=3.5) particles are almost the same as that of the pure Al₂O₃ particles (Fig. 6(a)). However, after explored by electron beam, a large amount of tiny particles can be found on the particle surface (Fig. 6(b)). It indicates that a thin layer of a second phase is formed homogeneously on the surface of Al₂O₃ nanoparticles, which is similar to that with urea as precipitant. With more NH₄HCO₃ solution adding (pH=6.8), the thickness of the second phase layer on the surface of Al₂O₃ nanoparticle increases (Fig. 6(c)). Simultaneously, some independent nanoparticles about 10–50 nm in diameter are noticed in the precursor. Based on the discussion before, these nanoparticles are identified as the self-assembled Y-compound. Compared with the Al₂O₃-Y(NO₃)₃-Urea system, the only difference in the reaction process of this Al₂O₃-Y(NO₃)₃-NH₄HCO₃ system lies in the slow reaction rate. As well known, the supersaturation, S , play a key role in chemical precipitation, and generally given by $S = a_A a_B / K_{sp}$, where a_A and a_B are the activities of the partially hydrolyzed cation (Y(H₂O)_x³⁺) and anion (CO₃²⁻), respectively; and K_{sp} is the solubility product constant.³⁴ Normally, when S reaches the critical supersaturation S^* , nucleation occurs. The low solubility product constants of Y₂(CO₃)₃ (1.03×10^{-31}) and Y(OH)₃ (1.00×10^{-22}) make it easy to reach supersaturation. By using urea as precipitant (Fig. 3), once the reaction temperature reaches 83 °C, a large amount of urea decompose, supplying sufficient precipitating ligands and reach very high supersaturation. Then, plenty of tiny Y-compound particles are formed which is defined as a burst nucleation process. Competed with this nucleation process, the nuclei are not prior to grow, but prior to assemble to lower the total surface energy. However, by using NH₄HCO₃ as precipitant (Fig. 7), the slow reaction process realizes a relatively low supersaturation leading to a small amount of Y-compound nuclei in the reaction system. These nuclei are prior to grow up with the proceeding of the reaction. The grown-up Y-compound nanoparticles supply new cores for the other Y-compound nanoparticles to assemble on, which is competitive to that of assembling on the precoated Al₂O₃ nanoparticles. Then, besides the increase of the Y-compound coating layer thickness, the individual Y-compound nanoparticles are formed in the system. Thus, in the Al₂O₃-Y(NO₃)₃-NH₄HCO₃ system, it is believed that the absence of burst nucleation process corresponds to the formation of individual Y-compound nanoparticles.

In general, the aforementioned results reveal that the formation of the core-shell structure by a partial wet process consists of two stages. First, the slow formation of Y-compound on the surface of the Al₂O₃ particles, which is initiated from the adsorption of Y ions and weak hydrolysis of urea. Second, plenty of tiny primary precipitate particles are formed in the suspension due to the burst nucleation process. Driven by the high surface energy of the nanoparticles, they assemble and form a shell structure on the precoated Al₂O₃ nanoparticles to lower the total surface energy. Different from the most familiar mechanism for the core-shell structure

formation³⁵⁻³⁷, in the burst nucleation process, the driven force is not only the traditional electrostatic attraction between the template-core and the shell materials, but also the high surface energy of the nanoparticles.

Conclusions

The mechanism of the core-shell structured yttrium-aluminum garnet (YAG) precursor formation is intensively studied. A two stages mechanism is proposed to describe this formation process. First, the surface of Al₂O₃ particles adsorb carbonate and hydroxyl groups and form some tiny Y-compound nuclei on the surface of Al₂O₃ nanoparticles before the burst nucleation occurring. Second, burst nucleation process occurs at urea decomposition temperature, and plenty of tiny Y-compound nuclei are formed simultaneously all over the suspension. By self-assembling of the Y-compound nanoparticles on the surface of the precoated Al₂O₃ nanoparticles, the Al₂O₃/Y-compound core-shell nanostructures are formed. During the most of the process, the electrostatic attraction between the opposite surface charges of Al₂O₃ and Y-compound nanoparticles is deemed as one apparent driven force. However, the high surface energy of Y-compound nanoparticles originated from the burst nucleation process plays a key role to complete the core-shell structure formation. Surface modification with negative charged PAA⁻ will block both the precoating process and assembling process, leading to the failure in the core-shell structure formation. By making the core-shell structure formation clear, the partial wet chemical route with a burst nucleation process can be applied on the morphology controllable synthesis of many other binary oxides.

Acknowledgements

This research was supported by an NSFC (NSFDYS: 50990303, 51372142, 51102040, 51402172), Innovation Research Group (IRG: 51321091), China Postdoctoral Science Foundation (2013M541909).

Notes

^a State Key Laboratory of Crystal Materials, Shandong University, 27 Shandan Road, Jinan, 250100, China

^b School of Materials and Metallurgy, Northeastern University, Shenyang, 110004, China

† These authors contribute equal to this work.

* Corresponding authors: sangyh@sdu.edu.cn (Y. Sang); hongliu@sdu.edu.cn (H. Liu)

Electronic Supplementary Information (ESI) available: the XRD patterns, the photographs of the as-obtained transparent ceramics, the pH evolution of different reaction system and the ICP-AES results of the residual ions in the solution after filtration. See DOI:

References

1 E. A. Ahmad, G. Mallia, D. Kramer, A. R. Kucernak and N. M. Harrison, *J. Mater. Chem. A*, 2013, **1**, 11152.

- 2 J. Griesbauer, T. Korner, T. Wehlius, A. Heinrich, B. Stritzker, J. Simon and W. Mader, *CrystEngComm*, 2011, **13**, 77.
- 3 J. G. Li, T. Ikegami, J. H. Lee, T. Mori and Y. Yajima, *J. Eur. Ceram. Soc.*, 2001, **21**, 139.
- 4 J. M. Patete, X. H. Peng, C. Koenigsmann, Y. Xu, B. Karn and S. S. Wong, *Green Chem.*, 2011, **13**, 482.
- 5 Y. D. Liu, J. Goebel and Y. D. Yin, *Chem. Soc. Rev.*, 2013, **42**, 2610.
- 6 M. Veith, S. Mathur, A. Kareiva, M. Jilavi, M. Zimmer and V. Huch, *J. Mater. Chem.*, 1999, **9**, 3069.
- 7 S. A. H. Tabrizi, E. T. Nassaj and H. Sarpoolaky, *J. Alloys Compd.*, 2008, **456**, 282.
- 8 X. J. Xu, X. D. Sun, H. Liu, J. G. Li, X. D. Li, D. Huo and S. H. Liu, *J. Am. Ceram. Soc.*, 2012, **95**, 3821.
- 9 D. J. Sordelet, M. Akinc, M. L. Panchula, Y. Han and M. H. Han, *J. Eur. Ceram. Soc.*, 1994, **14**, 123.
- 10 Y. J. Li, Y. C. Zhang and J. X. Leng, *Key Eng. Mater.*, 2014, 602-603, 110.
- 11 H. Z. Wang, L. Gao and K. Niihara, *Mater. Sci. Eng. A*, 2000, **288**, 1.
- 12 M. L. Saladino, G. Nasillo, D. C. Martino and E. Caponetti, *J. Alloys Compd.*, 2010, **491**, 737.
- 13 X. L. Zhang, D. Liu, Y. H. Sang, H. Liu and J. Y. Wang, *J. Alloys Compd.*, 2010, **502**, 206.
- 14 A. Aboulaich, J. Deschamps, R. Deloncle, A. Potdevin, B. Devouard, G. Chadeyron and R. Mahiou, *New J. Chem.*, 2012, **36**, 2493.
- 15 X. Li, H. Liu, J. Y. Wang, F. Han and R. I. Boughton, *J. Am. Ceram. Soc.*, 2004, **87**, 2288.
- 16 S. Bogatko and P. Geerlings, *Phys. Chem. Chem. Phys.*, 2012, **14**, 8058.
- 17 Y. H. Sang, H. Liu, X. D. Sun, X. L. Zhang, H. M. Qin, Y. H. Lv, D. Huo, D. Liu, J. Y. Wang and R. I. Boughton, *J. Alloys and Compd.*, 2011, **509**, 2407.
- 18 A. Sahraneshin, S. Takami, D. Hojo, T. Arita, K. Minami and T. Adschiri, *CrystEngComm*, 2012, **14**, 6085.
- 19 Y. H. Sang, Y. H. Lv, H. M. Qin, X. L. Zhang, H. Liu, J. Y. Wang, X. D. Sun and R. I. Boughton, *Ceram. Int*, 2012, **38**, 1635.
- 20 P. Palmero, C. Esnouf, L. Montanaro and G. Fantozzi, *J. Eur. Ceram. Soc.* 2005, **25**, 1565.
- 21 H. M. Qin, H. Liu, Y. H. Sang, Y. H. Lv, X. L. Zhang, Y. Y. Zhang, T. Ohachi, and J. Y. Wang, *CrystEngComm*, 2012, **14**, 1783.
- 22 H. M. Qin, X. H. Zhang, H. Liu, Y. H. Sang and J. Y. Wang, *CrystEngComm*, 2013, **15**, 5076.
- 23 M. Yao, W. M. Chen, X. Fan, C. M. Liu, X. M. Meng, L. Guo and C. P. Chen, *CrystEngComm*, 2011, **13**, 2593.
- 24 J. X. Yu, N. Du, H. Zhang and D. R. Yang, *RSC Adv.*, 2013, **3**, 7713.
- 25 G. Sahu, K. Wang, S. W. Gordon, W. L. Zhou and M. A. Tarr, *RSC Adv.*, 2012, **2**, 3791.
- 26 M. K. Han, X. W. Yin, L. Kong, M. Li, W. Y. Duan, L. T. Zhang and L. F. Cheng *J. Mater. Chem. A*, 2014, **2**, 16403.
- 27 Y. H. Sang, H. M. Qin, H. Liu, L. L. Zhao, Y. N. Wang, H. D. Jiang and J. Y. Wang, *J. Eur. Ceram. Soc.*, 2013, **33**, 2617.
- 28 J. G. Li, X. D. Li, X. D. Sun and I. Takamasa, *J. Phys. Chem. C*, 2008, **112**, 11707.
- 29 X. S. Li, V. K. Michaelis, T. C. Ong, S. J. Smith, I. McKay, P. Müller, R. G. Griffin and E. N. Wang, *CrystEngComm*, 2014, **16**, 2950.

- 30 J. Q. Jiao, X. Liu, W. Gao, C. W. Wang, H. J. Feng, X. L. Zhao and L. P. Chen, *CrystEngComm*, 2009, **11**, 1886.
- 31 N. Venkatachalam, Y. Saito and K. Soga, *J. Am. Ceram. Soc.*, 2009, **92**, 1006.
- 32 S. Som and S. K. Sharma, *J. Phys. D Appl. Phys.*, 2012, **45**, 415102.
- 33 V. K. Ivanov, A. E. Baranchikov, A. S. Vanetsev, A. S. Shaporev, O. S. Polezhaeva, Y. D. Tretyakov, P. P. Fedorov and V. V. Osiko, *Russ. J Inorg. Chem.*, 2007, **52**, 1321.
- 34 J. G. Li, X. Li, X. D. Sun, T. Ikegami and T. Ishigaki, *Chem. Mater.*, 2008, **20**, 2274-2281.
- 35 J. Geng, X. D. Jia and J. J. Zhu, *CrystEngComm*, 2011, **13**, 193.
- 36 D. A. Walker, B. Kowalczyk, M. O. de la Cruz and B. A. Grzybowski, *Nanoscale*, 2011, **3**, 1316.
- 37 J. F. L. Duval, J. Merlin and P. A. L. Narayana, *Phys. Chem. Chem. Phys.*, 2011, **13**, 1037.